



Framework to estimate the soil-water characteristic curve for soils with different void ratios

Qian Zhai¹ · Harianto Rahardjo² · Alfrendo Satyanaga² · Guoliang Dai¹ · Yan Zhuang¹

Received: 8 January 2020 / Accepted: 26 April 2020 / Published online: 8 May 2020
© Springer-Verlag GmbH Germany, part of Springer Nature 2020

Abstract

The soil-water characteristic curve (SWCC) contains information regarding the geometric pore space in a soil and is commonly used to estimate unsaturated soil properties, such as unsaturated hydraulic conductivity and unsaturated shear strength. Soil volume change can significantly affect the SWCC and the engineering properties of soil. Different SWCCs can be obtained if the soil specimens are prepared with different initial void ratios. The volumetric shrinkage curve (VSC) is commonly used to convert the SWCC in the form of gravimetric water content (w -SWCC) into a curve that is in the form of degree of saturation (S -SWCC). In this paper, a framework is developed in which different S -SWCCs are generated based on the measured w -SWCC of soil in a relatively loose condition and the VSC. The proposed framework is based on the concept of the pore size distribution function (PSDF). The estimated SWCCs corresponding to different initial void ratios from the proposed framework were verified by using experimental data from published studies.

Keywords Soil-water characteristic curve · Volumetric shrinkage curve · Pore-size distribution function · Framework · Soil volume change

Introduction

Different soil-water characteristic curves (SWCC) can be obtained if the soil specimens are prepared under different initial void ratios (Birle et al. 2008, Pham and Fredlund 2011; Gao et al. 2016 Gao and Sun 2017, Al-Dakheeli and Bulut 2019, Gao et al. 2019). Various models have been proposed for the

estimation of different SWCCs corresponding to different void ratios (Romero and Vaunat 2000; Sun et al. 2007; Zhou et al. 2012; Zhou et al. 2014; Zhou and Ng 2014; Mendes and Toll 2016; Wijaya and Leong 2017; Gao et al. 2019, and Roy and Rajesh 2020). Recently, the works from Fredlund and Houston (2013), Tripathy et al. (2002), Tripathy et al. (2014), Fredlund (2015), Fredlund (2017), and Lu and Dong (2017) advocated that the volumetric shrinkage curve (VSC) could be used to estimate the SWCC by considering the soil volume change.

It seems that the VSC has rarely been used for estimating the variation in the SWCC due to the changes in void ratio. In this paper, both the measured SWCC in the form of gravimetric water content (w -SWCC) and the VSC of soil in a loose condition are used as the input information for the estimation of the w -SWCCs of soil under different void ratios. The proposed methodology was verified with experimental data from published studies. The proposed framework provides an alternative method for the rapid estimation of the SWCC of soils with different void ratios.

✉ Qian Zhai
101012332@seu.edu.cn

Harianto Rahardjo
chrahardjo@ntu.edu.sg

Alfrendo Satyanaga
alfrendo@ntu.edu.sg

Guoliang Dai
daigl@seu.edu.cn

Yan Zhuang
Zhuangyan4444@hotmail.com

¹ Key Laboratory for RC and PRC Structures of the Ministry of Education, Southeast University, Nanjing 210096, China

² School of Civil and Environmental Engineering, Nanyang Technological University, Block N1, Nanyang Ave., Singapore 639798, Singapore

Literature review

The SWCC defines the relationship between soil suction and the amount of water in a soil. The amount of water in soil can be expressed in terms of the gravimetric water content, w ;

volumetric water content, θ ; or degree of saturation, S . Due to the different forms of expressing the amount of water in a soil, the SWCC can be expressed in terms of gravimetric water content, w -SWCC; volumetric water content, θ -SWCC; or degree of saturation, S -SWCC (Fredlund et al. 2018). Fredlund and Xing (1994) proposed the SWCC equation by integrating the assumed pore-size distribution function (PSDF), and the fitting parameters in the proposed equation are commonly determined from the regression analysis. If there is no soil volume change, then the w -SWCC that does not consider the soil volume change can be considered to represent the PSDF of the soil. However, if there is soil volume change, then the w -SWCC represents the PSDF of soil in the initial condition (which is in a loose condition), while the S -SWCC represents the PSDF of the soil in the final condition (which is in a dense condition). Zhai et al. (2018) showed that the PSDF also had a significant effect on the saturated coefficient of permeability for sandy soils.

Diamond (1970) suggested that there were two types of microstructures in a clayey soil, namely, relatively large-diameter pores and small-diameter pores with a dividing radius of 2000 Å. Romero et al. (1999) proposed an empirical method for dividing the pores in soil into “interaggregate zone” and “intra-aggregate zone” through the interpretation of Mercury Intrusion Porosimetry (MIP) test results. The experimental works of Delage and Lefebvre (1984), Griffiths and Joshi (1990), Kollijji et al. (2010), Han et al. (2017) and Han et al. (2019) showed that the changes in soil volume during compaction and consolidation are mainly due to the compression of interaggregate pores. Salager et al. (2013) indicated that the w -SWCCs for the same soil with different initial void ratios converged and became unique after certain suction values. As the SWCC at high suction ranges represents the micropores in soil, the variations in the initial void ratios would not change these micropores corresponding to the high suction levels. In addition, the works of Griffiths and Joshi (1990), Lapierre et al. (1990), Miao et al. (2007), Oualmakran et al. (2016), Sun and Cui (2017), and Li et al. (2018) showed that micropores were not compressed even when the applied load was large enough to destroy the interaggregate pores. As a result, it can be assumed that when the soil is subjected to compression (due to a mechanical load or suction load), the pores are compressed from the large pores to the small pores. The size range of the pores to be compressed is a function of the magnitude of the compression. Higher compression results in a wider size range of pores to be compressed.

The research works by Fredlund et al. (2002), Peng and Horn (2005), and Lin and Cerato (2013) showed that the VSC bears a relationship to the soil-water characteristic curve (SWCC) during drying from a near-saturated condition. Hamberg (1985) and Perko et al. (2000) proposed that the soil volume versus water content relationship under a free-

confining condition of drying be defined as a constitutive or characteristic curve. Volumetric shrinkage curves are commonly adopted to study the soil-water interaction and volumetric behavior of soils (McKeen 1992; Nelson and Miller 1992; Likos et al. 2003; Wijaya and Leong 2017). Fredlund and Houston (2013), Tripathy et al. (2014), Fredlund (2015), and Lu and Dong (2017) demonstrated that the VSC could be used to convert w -SWCC into S -SWCC. Tripathy et al. (2014) indicated that the water content of clay at the air-entry value was larger than the shrinkage limit of clay. Romero and Vaunat (2000) proposed a SWCC model by considering the variation in void ratio for expansive clay soils and collapsible clay soils.

In this paper, a framework that simulates the variations in the PSDF is proposed for the estimation of the SWCC of soils with different initial void ratios. As the proposed framework in this study is generated from the mathematical equations of the SWCC and VSC, both Fredlund and Xing's (1994) equation for the SWCC (Eq. 1) and Fredlund et al.'s (2002) equation for the VSC (Eq. 2) are adopted in this paper.

$$S = C(\psi) \frac{1}{\left\{ \ln \left[e + \left(\frac{\psi}{a_f} \right)^{n_f} \right] \right\}^{m_f}} = \left[1 - \frac{\ln \left(1 + \frac{\psi}{C_r} \right)}{\ln \left(1 + \frac{10^6}{C_r} \right)} \right] \frac{1}{\left\{ \ln \left[e + \left(\frac{\psi}{a_f} \right)^{n_f} \right] \right\}^{m_f}} \quad (1)$$

where a_f , n_f , m_f = fitting parameters for the S -SWCC equation and C_r = an input value related to the residual suction, which can be estimated as $C_r = 1500$ kPa for most cases (Fredlund and Xing 1994, Zhai and Rahardjo 2012 and Zhai et al. 2017a).

$$e = a_{sh} \left(\frac{W^{c_{sh}}}{b_{sh}^{c_{sh}}} + 1 \right)^{\frac{1}{c_{sh}}} \quad (2)$$

where a_{sh} = the minimum void ratio, b_{sh} = the slope of the line of tangency, and c_{sh} = the curvature of the shrinkage curve.

Theory

The relationship between the PSDF and SWCC is first explained for the case of a soil with a rigid soil structure during the SWCC measurement. Subsequently, the relationship between the PSDF and SWCC for a deformable soil is shown with consideration for the effects of soil volume change on the variation in the PSDF of the soil. Two major assumptions are adopted in the proposed framework: (i) the soil particles are not compressed during the compression of soil volume, and (ii) the pores in soils are compressed gradually from large

pores to smaller pores during the compression of soil volume. Consequently, a new PSDF-based framework for the estimation of SWCCs for soil with different initial water contents was proposed in this study.

Relationship between the PSDF and SWCC for a rigid soil

If the soil structure is rigid, the volume of water drained from the soil represents the dried volume of pores during the SWCC measurement. Based on the capillary law, the percentage of the volume of pores with particular pore sizes of r to $(r - \Delta r)$ can be obtained by measuring the water volume that drains out from the soil due to the increase in suction from ψ to $\Delta\psi$. The variable r is the pore radius, and ψ is the matric suction corresponding to the pore radius of r according to capillary law. The variables Δr and $\Delta\psi/r$ represent the change in pore radius and matric suction, respectively. The water volume associated with a variation in suction from ψ to $\Delta\psi$ represents the pore volume with pore sizes of r to $r - \Delta r$, which is the major assumption adopted by Fredlund and Xing (1994) in their derivation of a SWCC equation consistent with the concept of the pore-size distribution function.

The relationship between the PSDF and SWCC is shown in Fig. 1 (Zhai and Rahardjo 2015). Zhai and Rahardjo (2015) also explained that the S -SWCC could be divided into several segments, with each segment representing pores in the soil with the same radii. As shown in Fig. 1, the mean value of matric suction, ψ , for a segment represents the pore radius, r , (i.e., based on Kelvin’s capillary law) while the change in degree of saturation, ΔS , for the segment represents the pore-size density, $f(r)$, corresponding to the pores with radius of r . A detailed explanation of the relationship between the PSDF and SWCC for soil with a rigid soil structure can be found in Zhai and Rahardjo (2015) and Zhai et al. (2017b, 2018).

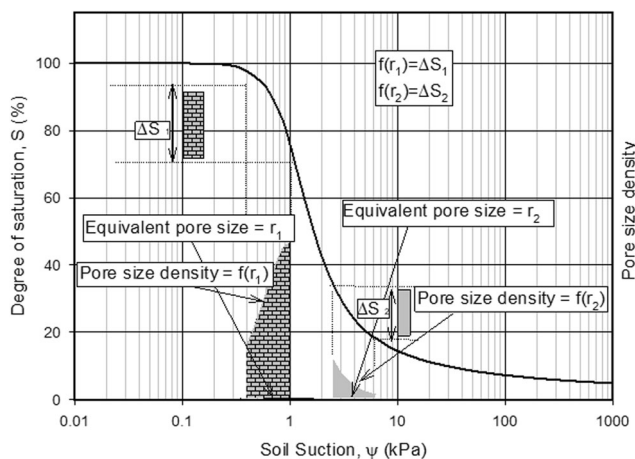


Fig. 1 Illustration of the relationship between PSDF and SWCC (modified from Zhai and Rahardjo 2015)

Relationship between the PSDF and SWCC for a deformable soil

Fredlund and Rahardjo (1993) explained that the difference between the pore-air pressure and pore-water pressure can be calculated from the radius of meniscus, based on the Young-Laplace equation, as shown in Fig. 2a, where T_s = the surface tension, T_v = the component of the surface tension in the y -direction, and T_h = the component of the surface tension in the x -direction. The relationship shown in Fig. 1 was based on the assumption that the soil structure remained rigid during the SWCC measurement. In other words, the relationship as explained in Fig. 1 may not be applicable for soils with significant changes in volume as soil suction changes. The volume change leads to the compression of large pores and a variation in the PSDF (i.e., the pore-size density for pores with different radii will redistribute if the large pores are compressed).

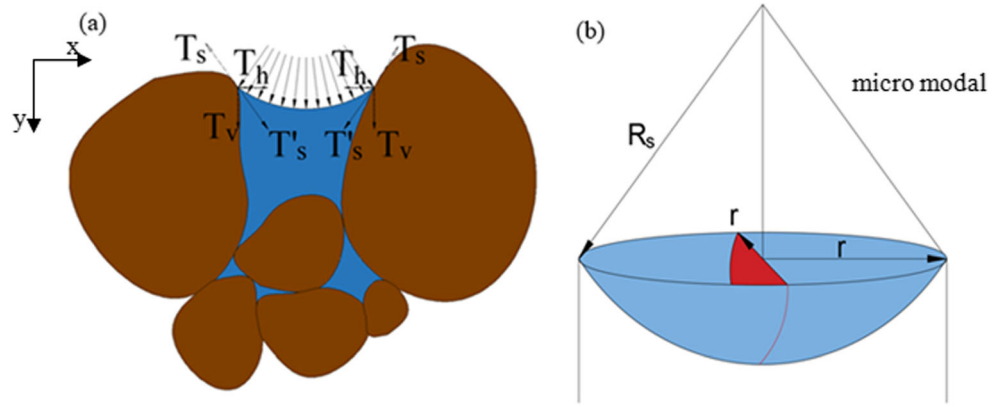
If the PSDF in a soil at an instantaneous state can be estimated, then a series of PSDFs corresponding to different instantaneous states can be used to represent the characteristics of the geometric pore space in the soil. In addition, for each instantaneous state, the relationship between the S -SWCC and PSDF, as shown in Fig. 1, is still valid because it can still be assumed that there is no soil volume change for an instantaneous state. As shown in Fig. 2, based on Newton’s second law, there will be a reactive force, T_s , acting on the soil particles if there is any surface tension, T_s , acting on the meniscus. As shown in Fig. 2, the decrease in pore radius, r , is dependent on the total horizontal pulling force between soil particles. Based on the geometrical relationship between the radii of the pore and meniscus shown in Fig. 2b, the total pulling force between soil particles can be calculated using Eq. (3) as follows:

$$P_F = (u_a - u_w)A' = (u_a - u_w) \left(R_s^2 \alpha - r \sqrt{R_s^2 - r^2} \right) \tag{3}$$

where P_F = the pulling force between soil particles; $(u_a - u_w)$ = matric suction; A' = the cross-sectional area of a spherical interior surface, as shown in Fig. 2b; R_s = the radius of the meniscus; r = the radius of the pore; and α = the angle defined by R_s and r . When r is notably smaller than R_s , the angle α can be approximately equal to $\sin\alpha$, which is equal to r/R_s . In this case, Eq. (3) can be simplified for the situation that r is much smaller than R_s as follows:

$$\begin{aligned} P_F &= (u_a - u_w) \left(R_s r - r \sqrt{R_s^2 - r^2} \right) \\ &= (u_a - u_w) R_s r \left(1 - \sqrt{1 - \left(\frac{r}{R_s} \right)^2} \right) \end{aligned} \tag{4}$$

Fig. 2 Illustration of meniscus and forces on the soil particles (modified from Zhai et al. 2019). **a** Force on soil particles. **b** Geometrical relationship between r and R_s



The details of the derivations of Eqs. (3) and (4) can be found in Zhai et al. (2019). If r is $\ll R_s$, then the term $1 - \sqrt{1 - (\frac{r}{R_s})^2}$ in Eq. (4) will be close to zero, which means that the pulling force between soil particles approaches zero. Therefore, if the pore size, r_i , is notably less than the equivalent pore size, r , corresponding to the applied suction, ψ , the variation in the suction will not cause any reduction in r_i .

If the entire geometrical pore space of soil is divided into n groups, then each group can be represented by a certain pore size with its statistical distribution. As shown in Fig. 3, the entire range of pore sizes with equivalent suctions from 0.01 kPa to 10^6 kPa are represented by only ten numbers of pores, and the pore radius can be considered notably larger than subsequent pores (i.e., $r_1 \gg r_2 \gg \dots \gg r_{10}$). As a result, when the suction increases to ψ_1 , some of the pores represented by r_1 will be compressed, and the pores with radii of r_2 to r_{10} will not be compressed. However, even though these pores with radii of r_2 to r_{10} are not compressed, the pore-size density of these pores will increase because the total volumes of pores are reduced due to the compression of pores with radius of r_1 . As a result, when the suction increases from 0.01 kPa to ψ_1 , the pore-size density of pores with a radius of r_1 will decrease, and the pore-size density of pores with radii of r_2 to r_{10} will increase with the same ratio of e_0/e_1 , as shown in Fig. 3.

Framework for the simulation of variation in the PSDF due to soil volume change

The degree of saturation, S , can be obtained when the water content and void ratio are known.

$$S = \frac{G_s w}{e} \tag{5}$$

where S = the degree of saturation, G_s = the specific gravity, w = the water content, and e = the void ratio. For a given soil, G_s always remains constant, and both w and e may vary under different states. The calculated degree of saturation for a given

measured water content may be different if a different void ratio is considered. As a result, the relationship between S_1 (corresponding to void ratio, e_1) and S_2 (corresponding to void ratio, e_2) can be defined by Eq. (6) as follows:

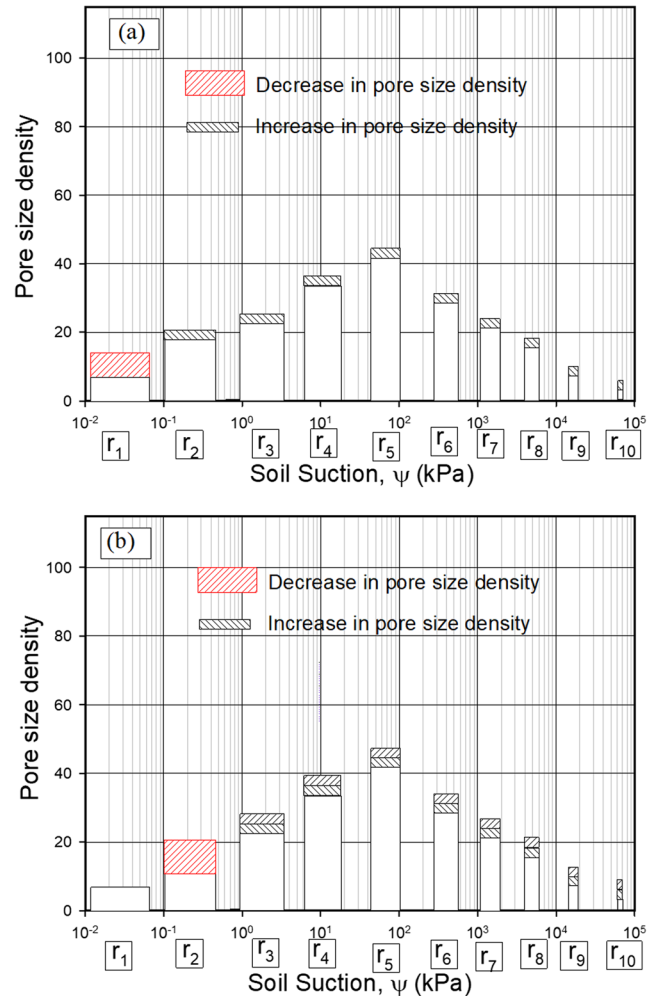


Fig. 3 Illustration of variation of pore-size densities of pores due to increase in soil suction. **a** Increase of soil suction from 0.01 kPa to ψ_1 . **b** Increase of soil suction from ψ_1 to ψ_2

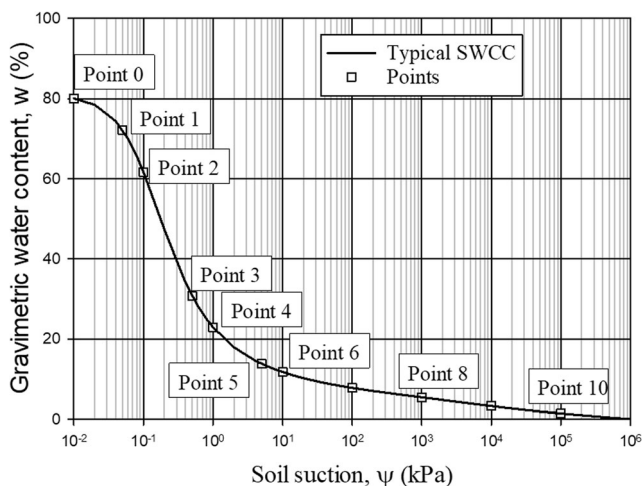


Fig. 4 Typical SWCC from Tempe cell/ Pressure Plate measurement ($a_f=0.1, n_f=1.5, m_f=1$)

$$\frac{S_1}{S_2} = \frac{e_2}{e_1} \tag{6}$$

where $S_1 = \frac{G_s w}{e_1}$ and $S_2 = \frac{G_s w}{e_2}$.

The converted S -SWCC can be shifted vertically by considering different void ratios, as shown in Eq. (6). The shifting of S -SWCC using Eq. (6) can be described as follows:

- (1) Divide the w -SWCC into several segments and name these as *points 0, 1, 2, 3* ———, as shown in Fig. 4.
- (2) Based on the point on the SWCC, divide the VSC accordingly, as shown in Fig. 5 (*point i* on the VSC has the same water content as *point i* on the w -SWCC).
- (3) Calculate the gravimetric water contents and void ratios for all the points on the w -SWCC and VSC, respectively.
- (4) Convert the gravimetric water contents ($w_0, w_1, w_2, w_3, \dots$) to corresponding degrees of saturation, S , by considering a constant void ratio of e_0 , and obtain $SWCC0$, which defines the PSDF for the soil with void ratio, e_0 .

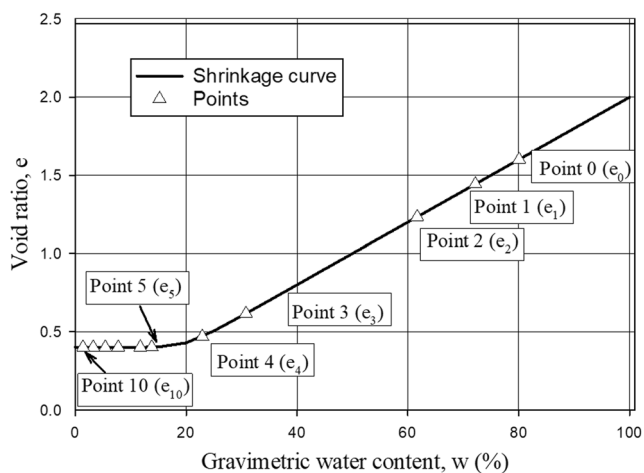


Fig. 5 Typical shrinkage curve ($a_{sh}=0.4, b_{sh}=0.2, c_{sh}=10$)

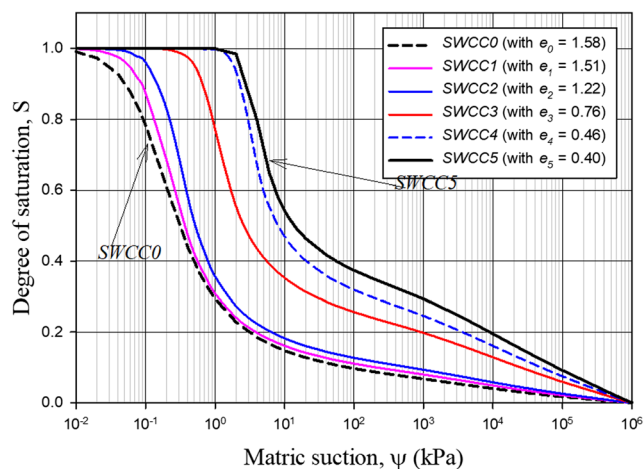


Fig. 6 Converted family of S -SWCCs

- (5) From *point 1*, convert the gravimetric water contents (w_1, w_2, w_3, \dots) to corresponding degrees of saturation, S , by considering a constant void ratio of e_1 and obtain $SWCC1$, which defines the PSDF for the soil with void ratio, e_1 .
- (6) From *point 2*, convert the gravimetric water contents (w_2, w_3, \dots) to corresponding degrees of saturation, S , by considering a constant void ratio, e_2 , and obtain $SWCC2$, which defines the PSDF for the soil with void ratio, e_2 .
- (7) Repeat steps (5) and (6) until the last point is reached.
- (8) Best-fit the converted degrees of saturation and generate the framework of the PSDF for a soil with different void ratios.

By following the steps described above, the conventional w -SWCC ($SWCC0$) is adopted to simulate the PSDF for the soil with an initial void ratio, which can be assumed to be in a relatively loose condition, while the converted S -SWCC

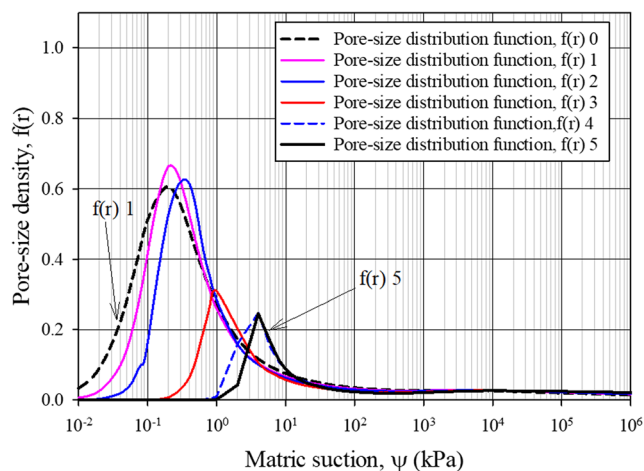


Fig. 7 Changes in pore-size distribution functions due to shrinkage of soil during the w -SWCC measurement

Table 1 Converted degrees of saturation

Points	Converted degrees of saturation					
	SWCC0	SWCC1	SWCC2	SWCC3	SWCC4	SWCC5
Point 0	$\frac{G_s w_0}{e_0}$	$\frac{G_s w_0}{e_0}$	$\frac{G_s w_0}{e_0}$	$\frac{G_s w_0}{e_0}$	$\frac{G_s w_0}{e_0}$	$\frac{G_s w_0}{e_0}$
Point 1	$\frac{G_s w_1}{e_0}$	$\frac{G_s w_1}{e_1}$	$\frac{G_s w_1}{e_1}$	$\frac{G_s w_1}{e_1}$	$\frac{G_s w_1}{e_1}$	$\frac{G_s w_1}{e_1}$
Point 2	$\frac{G_s w_2}{e_0}$	$\frac{G_s w_2}{e_1}$	$\frac{G_s w_2}{e_2}$	$\frac{G_s w_2}{e_2}$	$\frac{G_s w_2}{e_2}$	$\frac{G_s w_2}{e_2}$
Point 3	$\frac{G_s w_3}{e_0}$	$\frac{G_s w_3}{e_1}$	$\frac{G_s w_3}{e_2}$	$\frac{G_s w_3}{e_3}$	$\frac{G_s w_3}{e_3}$	$\frac{G_s w_3}{e_3}$
Point 4	$\frac{G_s w_4}{e_0}$	$\frac{G_s w_4}{e_1}$	$\frac{G_s w_4}{e_2}$	$\frac{G_s w_4}{e_3}$	$\frac{G_s w_4}{e_4}$	$\frac{G_s w_4}{e_4}$
Point 5	$\frac{G_s w_5}{e_0}$	$\frac{G_s w_5}{e_1}$	$\frac{G_s w_5}{e_2}$	$\frac{G_s w_5}{e_3}$	$\frac{G_s w_5}{e_4}$	$\frac{G_s w_5}{e_5}$
Point 6	$\frac{G_s w_6}{e_0}$	$\frac{G_s w_6}{e_1}$	$\frac{G_s w_6}{e_2}$	$\frac{G_s w_6}{e_3}$	$\frac{G_s w_6}{e_4}$	$\frac{G_s w_6}{e_5}$
Point 7	$\frac{G_s w_7}{e_0}$	$\frac{G_s w_7}{e_1}$	$\frac{G_s w_7}{e_2}$	$\frac{G_s w_7}{e_3}$	$\frac{G_s w_7}{e_4}$	$\frac{G_s w_7}{e_5}$
Point 8	$\frac{G_s w_8}{e_0}$	$\frac{G_s w_8}{e_1}$	$\frac{G_s w_8}{e_2}$	$\frac{G_s w_8}{e_3}$	$\frac{G_s w_8}{e_4}$	$\frac{G_s w_8}{e_5}$
Point 9	$\frac{G_s w_9}{e_0}$	$\frac{G_s w_9}{e_1}$	$\frac{G_s w_9}{e_2}$	$\frac{G_s w_9}{e_3}$	$\frac{G_s w_9}{e_4}$	$\frac{G_s w_9}{e_5}$
Point 10	$\frac{G_s w_{10}}{e_0}$	$\frac{G_s w_{10}}{e_1}$	$\frac{G_s w_{10}}{e_2}$	$\frac{G_s w_{10}}{e_3}$	$\frac{G_s w_{10}}{e_4}$	$\frac{G_s w_{10}}{e_5}$

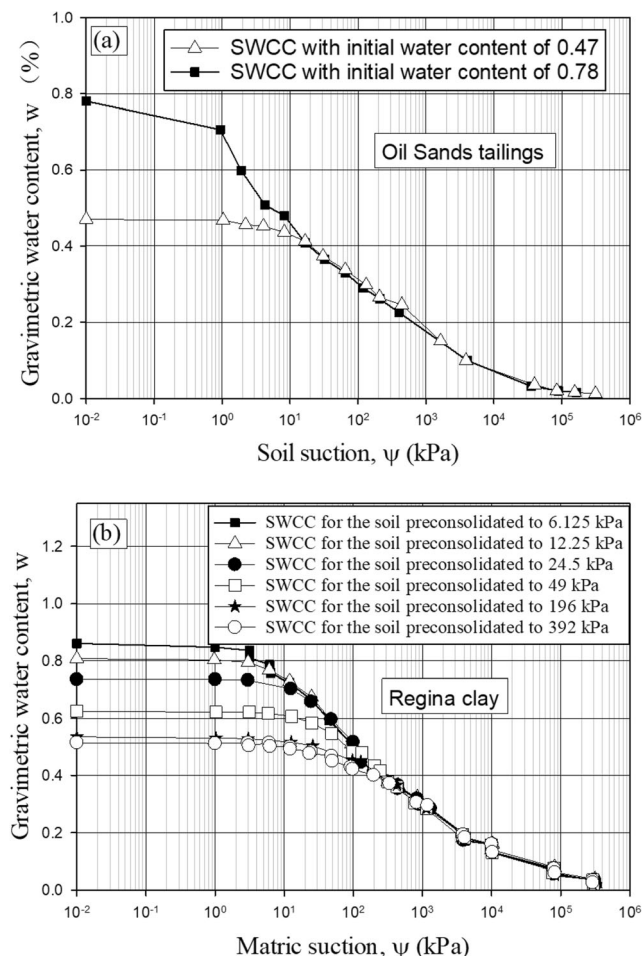


Fig. 8 Measured SWCCs for Oil Sands Tailings and Regina clay with different initial water contents. **a** Measured w -SWCCs for Oil Sands Tailings from Fredlund and Houston (2013). **b** Measured w -SWCCs for Regina clay from Fredlund (1964)

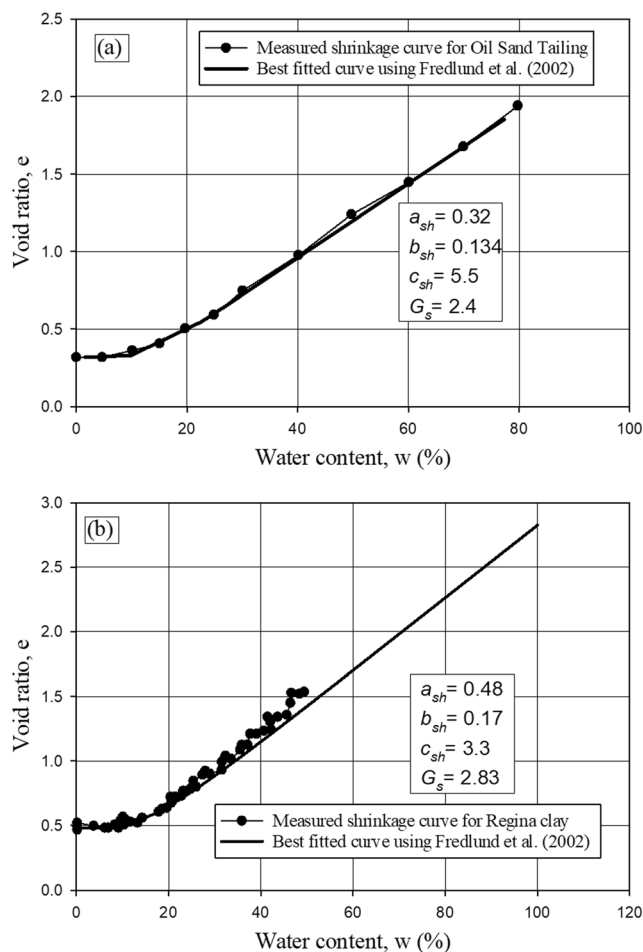


Fig. 9 Measured VSCs for Oil Sands Tailings and Regina clay from Fredlund and Houston (2013). **a** VSC for the Oil Sands Tailings. **b** VSC for the Regina clay

(*SWCC5*) is adopted to simulate the PSDF for the soil with the final void ratio, which is in a relatively dense condition, as shown in Figs. 6 and 7. Between *SWCC0* and *SWCC5*, *SWCC1* to *SWCC4* can be used to simulate the PSDFs of soils with different void ratios (i.e., e_1 to e_4).

Typical w -SWCCs obtained from soil with relatively loose conditions and VSCs were selected from the literature to demonstrate the steps involved in generating the proposed framework. As shown in Fig. 5, after point 5, the void ratio becomes constant. In this case, the PSDFs at points 5 to 10 will be the same because there is no soil volume change. Therefore, only one SWCC (i.e., *SWCC5*) is adopted to represent the PSDFs at points 5 to 10. The converted degrees of saturation for different SWCCs in the proposed framework from the measured w -SWCC data and VSC are shown in Table 1.

In Fig. 4, points 0 to 10 are evenly distributed within the suction range of [0.01 kPa, 1000 kPa]. As a result, the void ratios of e_0 to e_5 can be calculated from the VSC in Fig. 5 as [1.58, 1.51, 1.22, 0.76, 0.46, and 0.40]. A framework of PSDFs

(or a family of S -SWCCs) with the incorporation of soil volume change during w -SWCC measurement can be obtained as shown in Fig. 6. The S -SWCCs presented in Fig. 6 can be converted to the form of the PSDF following the procedure recommended by Zhai and Rahardjo (2015), as shown in Fig. 7.

Figure 6 shows that the converted SWCCs change from *SWCC0*, which represents the geometrical pore space in the soil at point 0 (initial stage), to *SWCC5*, which represents the geometrical pore space in the soil at point 10 (at the end of the SWCC test). Differential of curves in Fig. 6 gives the PSDFs of the soil, as shown in Fig. 7. Miao et al. (2007), Dieudonne et al. (2014), Oualmakran et al. (2016), Sun and Cui (2017), Gao et al. (2019), and Chamindu Deepagoda et al. (2019) reported similar results from the MIP tests.

Verification of the proposed framework

In the proposed framework, both the w -SWCC and VSC are required for the generation of the framework. The w -SWCCs of the soil with different initial water contents (or void ratios)

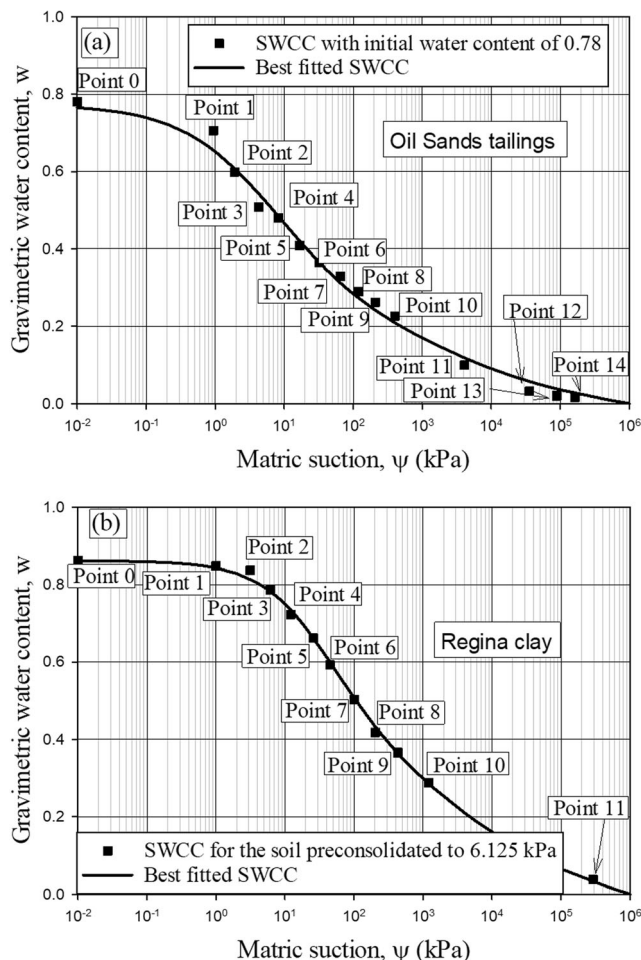


Fig. 10 Illustration of division of w -SWCC for the development of the framework for Oil Sands Tailings and Regina clay. **a** Selected points on w -SWCC for Oil Sands Tailings. **b** Selected points on w -SWCC for Regina clay

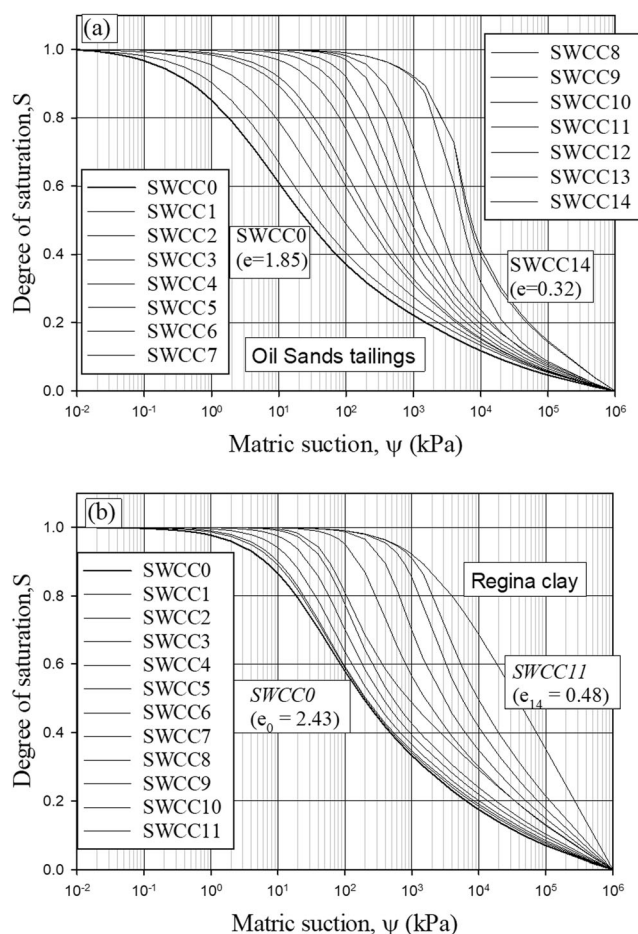


Fig. 11 Computed framework of SWCCs from measured w -SWCC and VSC for Oil Sands Tailings and Regina clay. **a** Framework of for the Oil Sands Tailings. **b** Framework of for the Regina clay

Table 2 Void ratios of soil corresponding to different SWCCs in the proposed framework

Family of <i>S</i> -SWCCs	Void ratio for Oil Sands tailings	Void ratio for Regina clay
SWCC0	1.85	2.43
SWCC1	1.69	2.40
SWCC2	1.44	2.36
SWCC3	1.22	2.23
SWCC4	1.15	2.05
SWCC5	0.98	1.88
SWCC6	0.87	1.68
SWCC7	0.79	1.43
SWCC8	0.70	1.20
SWCC9	0.63	1.06
SWCC10	0.55	0.85
SWCC11	0.33	0.48
SWCC12	0.32	–
SWCC13	0.32	–
SWCC14	0.32	–

can be used for the verification of the proposed framework. Based on the published literature, the experimental data on Oil Sands Tailings and Regina clay from Fredlund and Houston (2013) and Fredlund (1964) include information about both the *w*-SWCCs for soils with different initial water contents and shrinkage curves. As a result, both Oil Sands Tailings and Regina clay were selected in this study. The experimental data, which include the SWCC measurement and VSC of Oil Sands Tailings and Regina clay, are shown in Figs. 8 and 9, respectively.

Following the steps in the “[Framework for the simulation of variation in the PSDF due to soil volume change](#)” section, the SWCC of Oil Sands Tailings is divided into 15 segments (based on the measured data), and the SWCC of Regina clay is divided into 12 segments (based on the measured data), as shown in Fig. 10.

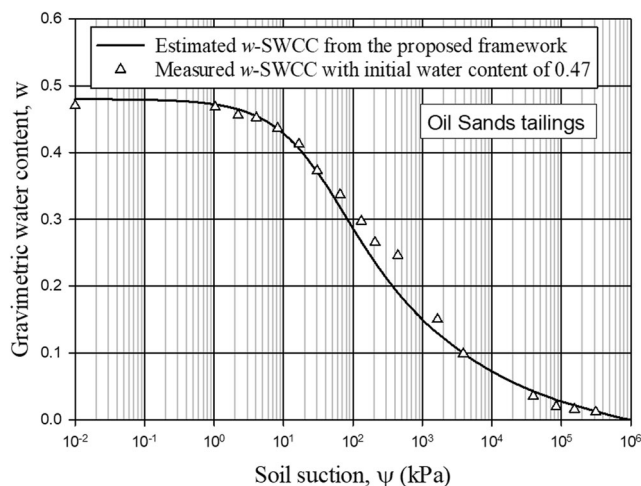


Fig. 12 Comparison between measured *w*-SWCC with initial water content of 0.47 and the estimation from proposed framework for Oil Sands Tailings

Converting the measured gravimetric water contents into degrees of saturation following the steps explained in the “[Framework for the simulation of variation in the PSDF due to soil volume change](#)” section and Table 1, the frameworks of the SWCCs for Oil Sands Tailings and Regina clay are finally obtained, as shown in Fig. 11.

The framework for the Oil Sands Tailings in Fig. 11a is obtained from the *w*-SWCC with an initial water content of 0.78 and the VSC, as shown in Fig. 9a. If the initial water content is 0.47, then the void ratio will be calculated as 1.13 from the VSC. The void ratio of 1.13 is mostly close to that corresponding to SWCC4 (which has an initial void ratio of 1.15), as shown in Table 2. In this case, SWCC4 is selected and multiplied by 0.48, which is calculated as the water content corresponding to the void ratio of 1.15. As a result, the estimated *w*-SWCC with an initial water content of 0.48 and measured *w*-SWCC with an initial water content of 0.47 are shown in Fig. 12.

The framework for Regina clay in Fig. 11b is obtained from the *w*-SWCC for the soil that has been preconsolidated to 6.13 kPa and the VSC, as shown in Fig. 9b. If the soil is preconsolidated to 12.25 kPa, the initial water content is 0.81, and the void ratio is calculated as 2.28 from the VSC. The void ratio of 2.28 is mostly close to those corresponding to SWCC2 and SWCC3 (which have initial void ratios of 2.36 and 2.23, respectively), as shown in Table 2. In this case, SWCC2 and SWCC3 are multiplied by 0.836 and 0.787, respectively, which are the calculated water contents corresponding to void ratios of 2.36 and 2.23, respectively. As a result, the estimated *w*-SWCC for the Regina clay and the measured *w*-SWCC for the specimen that has been preconsolidated to 12.25 kPa are shown in Fig. 13a. The initial water contents corresponding to the soil specimens preconsolidated to 24.5 kPa, 49 kPa, and 196 kPa were 0.74,

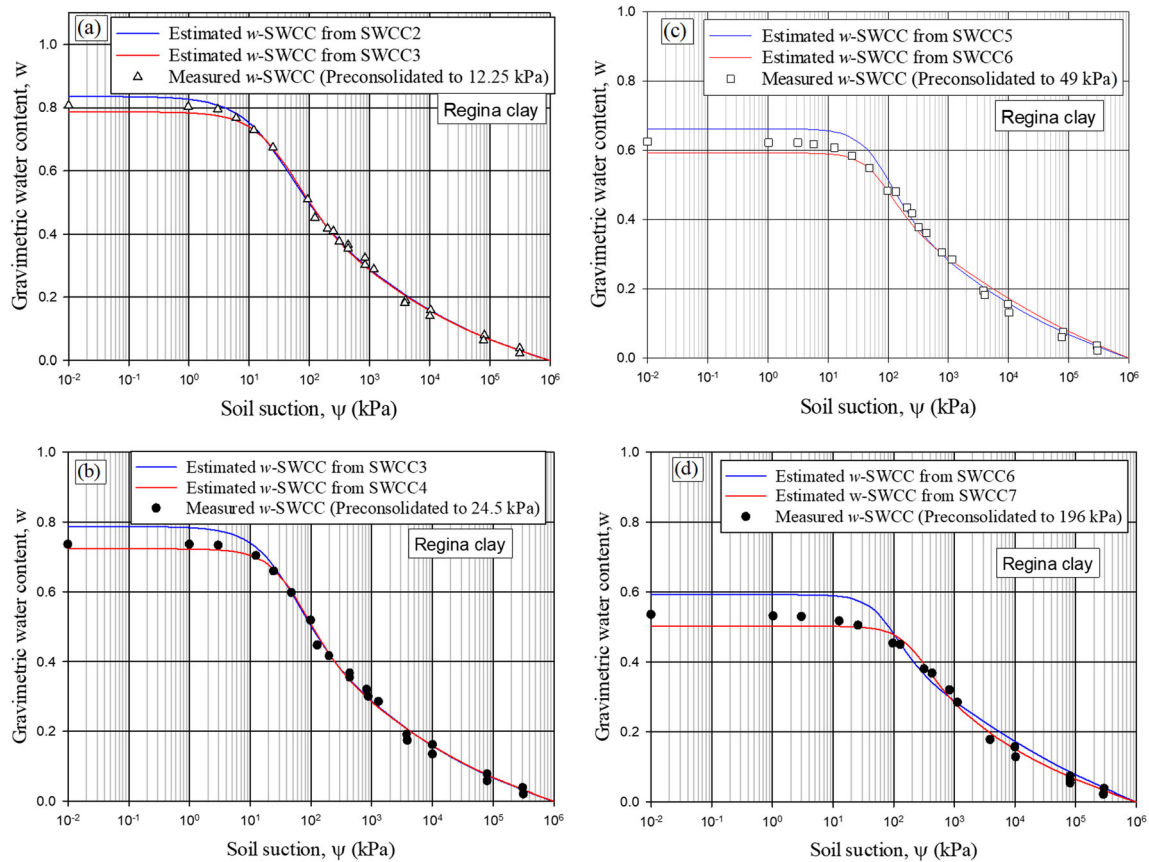


Fig. 13 Comparison between estimated w -SWCCs from the proposed framework and the measured w -SWCCs for Regina clay. **a** Soil is preconsolidated to 12.25 kPa. **b** Soil is preconsolidated to 24.5 kPa. **c** Soil is preconsolidated to 49 kPa. **d** Soil is preconsolidated to 196 kPa

0.63, and 0.54, and the calculated void ratios were 2.09, 1.79, and 1.53, respectively. Therefore, based on the void ratios shown in Table 2, *SWCC3* and *SWCC4* could be used to estimate the w -SWCC corresponding to the void ratio of 2.09, *SWCC5* and *SWCC6* could be used to estimate the w -SWCC corresponding to the void ratio of 1.79, and *SWCC6* and *SWCC7* could be used to estimate the w -SWCC corresponding to the void ratio of 1.53. Following similar procedures, the estimated w -SWCCs for the Regina clay and the measured w -SWCCs for the specimens that have been preconsolidated to 24.5 kPa, 49 kPa, and 196 kPa are shown in Fig. 13b–d, respectively.

Figures 12 and 13 show that the estimation of w -SWCCs using the concept of the PSDF agrees well with the measured SWCC data for Oil Sands Tailings and Regina clay. The comparison results indicate that the proposed framework can provide a good estimation of w -SWCCs with different initial saturated water contents (or void ratios).

Conclusions

A framework (in the form of S -SWCCs) with the incorporation of soil volume change has been proposed. The

methodology and procedure to develop the proposed framework have been explained and demonstrated. The experimental data for both Oil Sands Tailings and Regina clay from the literature show good agreement with the estimation results obtained from the proposed framework. The proposed framework is developed based on the concept of the pore-size distribution function. The proposed framework provides an alternative method for the estimation of SWCCs for soils with different void ratios. The proposed framework is based on the assumption that soil particles are not compressed during the variation in void ratios. Further research incorporating the compression of soil particles is warranted.

Funding information The first author would like to acknowledge the financial supports he received from the National Natural Science Foundation of China (No. 51878160), the National Key Research and development program of China (No. 2017YFC00703408), and the Research Funding from China Huaneng Group Co. Ltd. (HNKJ19-H17).

References

Al-Dakheeli H, Bulut R (2019) Interrelationship between elastic deformation and soil-water characteristic curve of expansive soils. *J Geotech Geoenviron* 145(4):04019005

- Birle E, Heyer D, Vogt N (2008) Influence of the initial water content and dry density on the soil–water retention curve and the shrinkage behavior of a compacted clay. *Acta Geotech* 3(3):191–200
- Chamindu Deepagoda TKK, Jayarathne JRRN, Clough TJ, Thomas S, Elberling B (2019) Soil-gas diffusivity and soil-moisture effects on N₂O emissions from intact pasture soils. *Soil Sci Soc Am J* 83: 1032–1043
- Delage P, Lefebvre G (1984) Study of the structure of a sensitive Champlain clay and its evolution during consolidation. *Can Geotech J* 21(1):21–35
- Diamond (1970) Pore size distributions in clay. *Clay Clay Miner* 18:7–23
- Dieudonne AC, Della Vecchia G, Charlier R, and Jommi C (2014) “Influence of microfabric evolution on the retention behavior of compacted clayey soils”, Proceedings of 6th International Conference on Unsaturated Soils, UNSAT, Sydney, Australia, pp: 679–684
- Fredlund, D.G. (1964) “Comparison of soil suction and one-dimensional consolidation characteristics of a highly plastic clay.” National Research Council of Canada, Division of Building Research, Technical Report No. 245, Ottawa, Ontario, Canada
- Fredlund, D.G. (2015) “Relationship between the laboratory SWCCs and field stress state”, proceeding of UNSAT 2015. Guilin, China, 23–26-October
- Fredlund DG (2017) “Role of the soil-water characteristic curve in unsaturated soil mechanics”, ICSMGE 2017 - 19th International Conference on Soil Mechanics and Geotechnical Engineering, p 57–79, 2017, ICSMGE 2017 - 19th International Conference on Soil Mechanics and Geotechnical Engineering
- Fredlund, D.G., Rahardjo, H., and Fredlund, M.D. (2018). Understanding the family of soil-water characteristic curves”, Proceedings of the Canadian Geotechnical Conference, Sept. 23–26, Edmonton, AB, geo2018, Paper 395
- Fredlund, D.G. and Houston S.L. (2013) “Interpretation of soil-water characteristic curves when volume change occurs as soil suction is changed” advances in unsaturated soils - proceedings of the 1st pan-American conference on unsaturated soils, PanAmUNSAT 2013, p 15–31, 2013, advances in unsaturated soils - proceedings of the 1st pan-American conference on unsaturated soils, PanAmUNSAT 2013
- Fredlund DG, Rahardjo H (1993) *Soil mechanics for unsaturated soil*. Wiley, New York, N.Y
- Fredlund DG, Xing A (1994) Equations for the soil-water characteristic curve. *Can Geotech J* 31(3):521–532
- Fredlund, M. D., Wilson, G. W., and Fredlund, D. G. (2002). “Representation and estimation of the shrinkage curve.” Proc., 3rd Int. Conf. On unsaturated soils, UNSAT 2002, Recife, Brazil, pp. 145–149
- Gao Y, Sun DA, Zhou AN (2016) Hydro-mechanical behaviour of unsaturated soil with different specimen preparations. *Can Geotech J* 53(6):1–9
- Gao Y, Sun D (2017) Soil-water retention behavior of compacted soil with different densities over a wide suction range and its prediction. *Comput Geotech* 91:17–26
- Gao Y, Sun D, Zhu ZC, Xu YF (2019) Hydromechanical behavior of unsaturated soil with different initial densities over a wide suction range. *Acta Geotech* 14(2):417–428
- Griffiths FJ, Joshi RC (1990) Change in pore size distribution due to consolidation of clays. *Geotechnique* 40(2):303–309
- Hamberg, D. J. (1985). “A simplified method for predicting heave in expansive soils.” M.S. thesis, Colorado State Univ., Fort Collins, CO.
- Han, Z., Vanapalli, S. K.*, and Zou, W. -L. (2017). Integrated approaches for predicting soil-water characteristic curve and resilient modulus of compacted subgrade soils. *Can Geotech J* 54(5):646–663.
- Han, Z., Vanapalli, S.K., Zou, W.L., Wang, X.Q., Zhang, J.F. (2019) Modelling virgin compression line of compacted unsaturated soils. *Acta Geotech* 14(6):1991–2006
- Kolliji A, Vulliet L, Laloui L (2010) Structural characterization of unsaturated aggregated soil. *Can Geotech J* 47(3):297–311
- Lapierre C, Leroueil S, Locat J (1990) Mercury intrusion and permeability of Louisville clay. *Can Geotech J* 27(6):761–773. <https://doi.org/10.1139/t90-090>
- Li ZS, Benchouk A, Derfouf FEM, Abou-Bekr N, Taibi S, Souli H, Fleureau JM (2018) Global representation of the drying–wetting curves of four engineering soils: experiments and correlations. *Acta Geotech* 13:51–71
- Likos, W. J., Olsen, H. W., Krosley, L., and Lu, N. (2003). “Measured and estimated suction indices for swelling potential classification.” *J Geotech Geoenviron Eng*, [https://doi.org/10.1061/\(ASCE\)1090-0241\(2003\)129:7\(665\)](https://doi.org/10.1061/(ASCE)1090-0241(2003)129:7(665)), pp. 665–668
- Lin B, Cerato AB (2013) Hysteretic soil water characteristics and cyclic swell–shrink paths of compacted expansive soils. *Bull Eng Geol Environ* 72(1):61–70
- Lu N, Dong Y (2017) Correlation between soil-shrinkage curve and water-retention characteristics. *J Geotech Geoenviron* 143(9): 04017054
- McKeen, R. G. (1992). “A model for predicting expansive soil behavior.” Proc., 7th Int. Conf. On expansive soils, pp. 1–6
- Mendes JD, Toll G (2016) Influence of initial water content on the mechanical behavior of unsaturated sandy clay soil. *Int J Geomech* 16(6):D4016005
- Miao L, Houston SL, Cui Y, Yuan J (2007) Relationship between soil structure and mechanical behavior for an expansive unsaturated clay. *Can Geotech J* 44(2):126–137
- Nelson JD, Miller DJ (1992) *Expansive soils: problem and practice in foundation and pavement engineering*. John Wiley, New York, N.Y
- Oualmakran M, Mercatoris BCN, Francois B (2016) Pore-size distribution of a compacted silty soil after compaction, saturation, and loading. *Can Geotech J* 53(12):1902–1909
- Pham HQ, Fredlund DG (2011) Volume-mass unsaturated soil constitutive model for drying-wetting under isotropic loading- unloading conditions. *Can Geotech J* 48(2):280–313
- Peng X, Horn R (2005) Modeling soil shrinkage curve across a wide range of soil types. *Soil Sci Soc Am J* 69(3):584–592
- Perko HA, Thompson RW, Nelson JD (2000) Suction compression index based on CLOD test results. *Advances in unsaturated geotechnics*, C. D
- Romero E, Gens A, Lloret A (1999) Water permeability, water retention and microstructure of unsaturated boom clay. *Eng Geol* 54:117–127
- Romero, E. & Vaunat, J. (2000). “Retention curves of deformable clays. In Experimental evidence and theoretical approaches in unsaturated soils” (eds A. Tarantino A. and C. Mancuso), proceedings of an international workshop on unsaturated soils, Trento, Italy, pp. 91–106. Rotterdam: AA Balkema
- Roy S, Rajesh S (2020) Simplified model to predict features of soil-water retention curve accounting for stress state condition. *Int J Geomech* 20(3):04019191
- Salager S, Nuth M, Ferrari A, Laloui L (2013) Investigation into water retention behaviour of deformable soils. *Can Geotech J* 50(2):200–208
- Sun DA, Sheng DC, Xu YF (2007) Collapse behaviour of unsaturated compacted soil with different initial densities. *Can Geotech J* 44(6): 673–686
- Sun WJ, Cui YJ (2017) Investigating the microstructure changes for silty soil during drying. *Geotechnique* 68(4):370–373
- Tripathy S, Subba K, Fredlund DG (2002) Water content-void ratio swell-shrink paths of compacted expansive soils. *Can Geotech J* 39:938–959
- Tripathy S, Tadza MYM, Thomas HR (2014) Soil-water characteristic curves of clays. *Can Geotech J* 51(8):869–883

- Wijaya M, Leong EC (2017) Modelling the effect of density on the unimodal soil-water characteristic curve. *Géotechnique* 67(7):637–645
- Zhai Q, Rahardjo H (2012) Determination of soil–water characteristic curve variables. *Computer Geotechnique* No 42:37–43
- Zhai Q, Rahardjo H (2015) Estimation of permeability function from soil-water characteristic curve. *Eng Geol* 199:148–156
- Zhai Q, Rahardjo H, Satyanaga A (2017a) Effects of residual suction and residual water content on the estimation of permeability. *Geoderma* 303:165–177
- Zhai Q, Rahardjo H, Satyanaga A (2017b) Effect of bimodal soil-water characteristic curve on the estimation of permeability function. *Eng Geol* 230:142–151
- Zhai Q, Rahardjo H, Satyanaga A (2018) The pore-size distribution framework for the estimation of hydraulic properties for sandy soil. *Eng Geol* 246:288–292
- Zhai Q, Rahardjo H, Satyanaga A, Dai GL (2019) Estimation of unsaturated shear strength from soil-water characteristic curve. *Acta Geotech* 14(6):1977–1990
- Zhou, A. N., Sheng, D. & Carter, J. P. (2012). “Modelling the effect of initial density on soil-water characteristic curves.” *Géotechnique* 62, No. 8, 669–680, <https://doi.org/10.1680/geot.10.P.120>
- Zhou C, Ng CWW (2014) A new and simple stress-dependent water retention model for unsaturated soil. *Comput Geotech* 62:216–222
- Zhou WH, Yuen KV, Tan F (2014) Estimation of soil–water characteristic curve and relative permeability for granular soils with different initial dry densities. *Eng Geol* 179:1–9